A Journal of the Gesellschaft Deutscher Chemiker
Angewandte
GDCh
International Edition
Chemie
www.angewandte.org

Accepted Article

Title: Robust Supramolecular Nano-tunnels Built from Molecular Bricks

Authors: Peifa Wei, Xuan He, Zheng Zheng, Donglin He, Qiyao Li, Junyi Gong, Jun Zhang, Herman H. Y. Sung, Ian D. Williams, Jacky W. Y. Lam, Ming Liu, and Ben Zhong Tang

To be cited as: *Angew. Chem. Int. Ed.* 10.1002/anie.202013117

Link to VoR: https://doi.org/10.1002/anie.202013117

WILEY-VCH

10.1002/anie.202013117

WILEY-VCH

RESEARCH ARTICLE

Robust Supramolecular Nano-tunnels Built from Molecular Bricks

Peifa Wei,*[a][b] Xuan He,[b] Zheng Zheng,[a] Donglin He,[c] Qiyao Li,[a] Junyi Gong,[a] Jun Zhang,[a] Herman H. Y. Sung,[a] Ian D. Williams,[a] Jacky W. Y. Lam,[a] Ming Liu,*[c] and Ben Zhong Tang*[a][d]

Abstract: Chemists are always seeking new methods to construct porous lattice frameworks from simple motifs. To date, the most common tectons of reported porous frameworks are predesigned multi-armed scaffolds with C_3, C_4 or C_6 symmetry. Linear two-armed tectons with C_2 symmetry are easier to synthesize but cannot form porous architectures by themself, unless combined with tectons of different symmetry. Herein we report a linear ionic molecule that assembles into a supramolecular nano-tunnel structure through synergy of trident-type ionic interactions and π-π stacking interactions. The nano-tunnel crystal exhibits anisotropic guest adsorption behavior. The material shows good thermal stability and undergoes multi-stage single-crystal-to-single-crystal phase transformations to a nonporous structure on heating. The material exhibits remarkable chemical stability in both acidic and basic conditions, which is rarely observed in supramolecular organic frameworks and is often related to structures with designed hydrogen bonding interactions. Because of the high polarity of the tunnels, this molecular crystal also shows a large CO_2 adsorption capacity while excluding other gases at ambient temperature, leading to high CO_2/CH_4 selectivity. The aggregation-induced emission feature of the molecules gives the bulk crystals vapochromic behavior.

Introduction

Nature is unrivaled in its ability to create structural complexity from small organic molecules.[1] Chemists have always been pursuing the virtue of simplicity in constructing functional structures using simple motifs, with the benefit of readily synthetic feasibility and structural tunability.[2] Porous crystalline solids of small organic molecules, constructed exclusively via non-covalent interactions, have emerged as an attractive type of porous materials in the past two decades after being first proposed in 1976.[3] Some organic molecular crystals exhibit porosity that rivals extended frameworks such as metal–organic frameworks and covalent organic frameworks.[4] Obtaining robust porous molecular crystals from simple tectons relies on ingenious molecular design.[5] The topology of the tectons should be geometrically favorable for the formation of stable framework with "virtual porosity"[6] by maximizing the interactions with minimum contact points. With regard to the shape and symmetry factor, predesigned multi-armed scaffolds with C_3, C_4 or C_6 symmetry protruding radially produce directional interactions in space to direct pore formation (Scheme S1).[7] Linear C_2 symmetric tectons are easier to synthesize, but cannot form architectures with open pores unless combined with building blocks of different symmetry.[8]

Linkage interactions that are strong enough to stabilize supramolecular frameworks formed by organic molecules are still limited. Hydrogen (H)-bonding is by far the most successful one to construct such frameworks, which has led to the rise of the field of H-bonding Organic Frameworks (HOFs) and Supramolecular Organic Frameworks (SOFs).[7, 9] Among these H-bonded frameworks, Miljanić, Aida, Schröder and others reported a few examples that exhibited good thermal and chemical stability which are rarely seen in organic crystalline porous solids.[9] However, such systems are often limited to specific functional groups that contribute to H-bonding interaction, and the resulting systems are labile to solvents that can interfere with H-bond formation.[7b, 7c] Apart from H-bonding, ionic interactions have proven to be good to methodically regulate molecular arrangements and construct stable ionic frameworks. A large number of crystalline porous organic salts have since been reported, pioneerred by Tohnai[10], Comotti[10c, 10d] and Ward[11], including elegant nanoporous structures from pairs of charged components, such as protonated amines or guanidinium cations with sulfonate anions. However, most reported examples can not retain their permanent porosity after removal of guest molecules.[10c, 10d, 12]

Here we report a linear ionic molecule that can form a stable framework with open pores through *X*-aggregation packing, facilitated by a combination of trident-type ionic interactions and π-π stacking interactions. The bulk crystal exhibits anisotropic guest diffusion behavior, which originates from the confined nano-tunnel type pores in the formed framework. The nano-tunnel crystal exhibits remarkable chemical stability in both acidic and basic conditions. Moreover, benefiting from the high polarity of the tunnels, this molecular crystal also shows a large CO_2 adsorption capacity and high CO_2/CH_4 selectivity at room temperature. Noteworthily, the linear cyanostilbene-based tecton is a readily accessible aggregation-induced emission (AIE) fluorophore, which gives the bulk crystals vapochromic behavior.[13]

[a] Prof. P. Wei, Dr. Z. Zheng, Q. Li, J. Gong, J. Zhang, Dr. H. H. Y. Sung, Prof. I. D. Williams, Dr. J. W. Y. Lam, Prof. B. Z. Tang
Department of Chemistry, The Hong Kong Branch of Chinese National Engineering Research Center for Tissue Restoration and Reconstruction, SCUT-HKUST Joint Research Institute, Institute for Advanced Study, Department of Chemical and Biological Engineering, The Hong Kong University of Science and Technology, Clear Water Bay, Kowloon, Hong Kong, China
Email: tangbenz@ust.hk; pfwei@ahu.edu.cn
[b] Prof. P. Wei, X. He
Institutes of Physical Science and Information Technology, Anhui University, Hefei 230601, China
[c] D. He, Dr. M. Liu
Materials Innovation Factory and Department of Chemistry, University of Liverpool, 51 Oxford Street, Liverpool, L7 3NY, United Kingdom
Email: Ming.Liu@liverpool.ac.uk
[d] Prof. B. Z. Tang
Center for Aggregation-Induced Emission, State Key Laboratory of Luminescent Materials and Devices, South China University of Technology, Guangzhou, 510640, China

Supporting information for this article is given via a link at the end of the document.

10.1002/anie.202013117

Results and Discussion

Structural Analysis of the Ionic Crystals with Open-pore Structure. Paraquat is a well-known planar electron-acceptor and dicyanostilbene is an AIE fluorophore with twisted conformation. By connecting these two units, we designed a new molecule, (*E*)-4,4'-((1,2-dicyanoethene-1,2-diyl)bis(4,1-phenylene))bis(1-methylpyridin-1-ium) hexafluorophosphate (**PCS**), which can be prepared in gram-scale via a four-step synthetic route (Figures 1a and S1-S4 and Scheme S2). **PCS** is a dication molecule with its charge balanced originally by two I_3^- ions, as confirmed by its single crystal structure (**PCS-I**, Figure S10), and latter by two PF_6^- ions (Scheme S2). Hexagonal-prism shaped single crystals of **PCS** (**PCS^S**), can be readily obtained by slow vapor diffusion of diisopropyl ether into acetonitrile solution. **PCS^S** shows one-dimensional (1D) pores with a diameter of ~ 6.2 Å and the solvents trapped inside are identified as acetonitrile and diisopropyl ether by ^{1}H NMR spectroscopy (Figure S31c). The single crystal data of **PCS^S** reveals that each **PCS** molecule consists of two crystallographically distinct arms: the four aromatic rings on the two arms twist in different angles out of the plane of the central dicyanoethylene molecule (Figure S7). Meanwhile, the electrostatic potential diagram (Figure S8) suggests the organic part of **PCS** is a rather electron deficient moiety. The twisted molecular conformation, in combination with the absence of electron donor, disfavors the perfect packing between two PCS molecules, which play a key role in creating pores in molecular crystals (Figure 1g-h). Interestingly, in the structure, each PF_6^- anion can act as a joint that interacts with up to five **PCS** molecules through multiple C-H…F and F…π interactions with distances in the range of 2.14 – 3.16 Å (Figures 1h and S9). Each PF_6^- counterion acts as a trident anion to connect three **PCS** at three adjacent layers to form a stable three-armed supramolecular tecton, which is similar to a C_3-symmetric building block in chemistry of frameworks.[9b] Two C_3-type supramolecular tectons can then arrange in a brickwork way to form dumbbell-type units (Figure 1e-f) whose further propagation forms a three-dimensional (3D) structure (Figure 1b-d). While for the precursor **PCS** with I_3^- ions, a dense packing structure was observed (Figure S10), which indicates the critical role of PF_6^- in forming a stable porous structure. Density functional theory calculation was used to evaluate the effect of packing angles (θ) of **PCS** molecules on the system energy. The result suggests that the system energy reaches its minimum at θ = 128º, which is very close to the *X*-aggregation packing mode (θ = 120º) we observed in the **PCS** crystal (Figure S11). "Virtual porosity" was observed in the crystal structure, with a total solvent-accessible void at 26.2% of its volume estimated by *PLATON* analysis (Figure S12) using a 1.2 Å probe.[14]

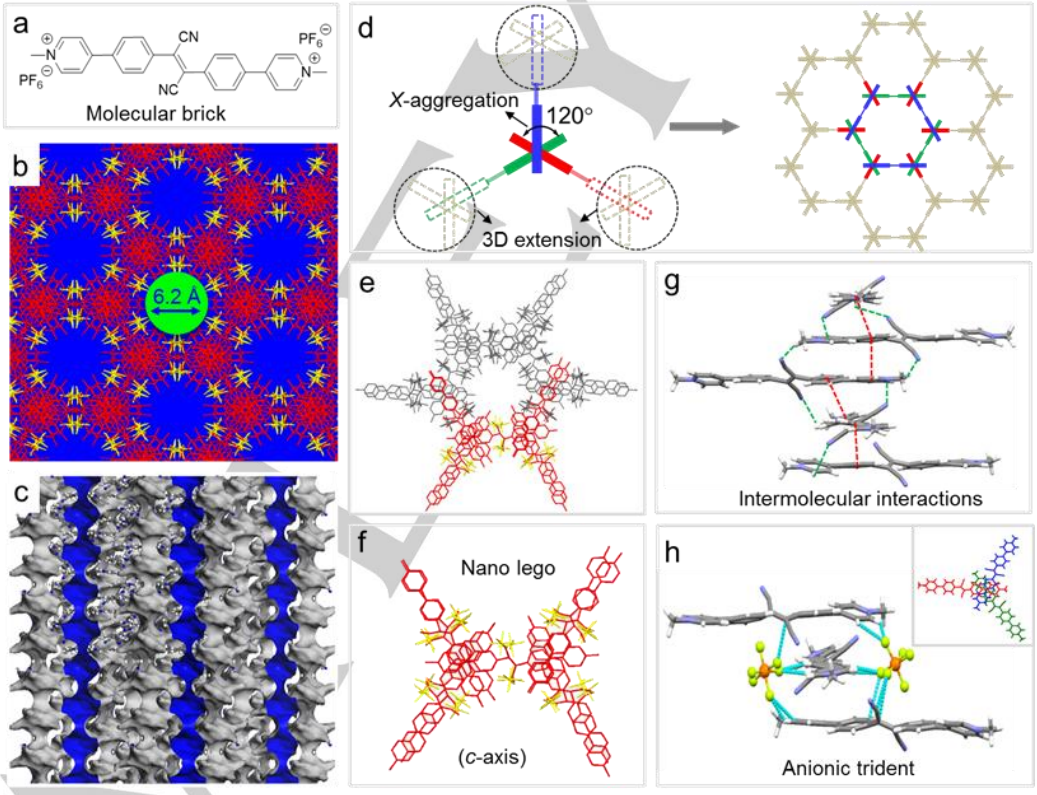

Figure 1. (a) Molecular structure of **PCS**. (b) The honeycomb like tunnel structure viewed along *c*-axis in capped-stick representation. (c) The smoothed solvent accessible surfaces created using *Materials Studio*, and the structures have then been sliced along the *c*-axis. (d) The cartoon representation of the formation of tunnels. (e) Crystal packing along the *c*-axis of the hexagonal framework of the tunnel. (f) The minimum repeating units of the crystal lattice along the *c*-axis. (g) Intermolecular interactions. The green dashed lines indicate intermolecular C-H...N hydrogen bonding with a distance of less than 2.90 Å. The red dashed line indicated intermolecular π-π interactions. (h) The trident anion (view along the *a*-axis) that stabilizes the tunnel. The cyan dashed lines indicate F...π and C-H...F interactions between PF_6^- and **PCS**. PF_6^- in (c), (e) and (g) was omitted for clarity.

10.1002/anie.202013117

Anisotropic Iodine Diffusion in PCS Crystal. Although a crystalline porous solid with 1D channels is not unusual, very few examples have shown bulk anisotropic adsorption behavior.[15] **PCS** molecules exhibit AIE behavior, as proven by their weak emission in a good solvent (acetonitrile) and enhanced photoluminescence (PL) in a poor solvent (diisopropyl ether) (Figure S13). **PCS^S** is clear yellow and shows blue-green emission when irradiated with 365 nm UV light (Figure 2c). This inspires us to check whether **PCS^S** can exhibit colour or fluorescence changes after adsorbing guest molecules. If this is the case, this feature can thus be used as a tool to probe the existence of 1D channels in the bulk crystals. I_2 was chosen due to its strong fluorescent quenching effect for monitoring the diffusion process.[16] **PCS^S** was placed in a vial and then exposed to iodine vapor in a sealed container at room temperature. After a few seconds, staining starts to appear at both the ends of the crystal, which are attributed to the (001) faces of the hexagonal prism (Figure 2a). The staining gradually reaches the central part of the crystal and the whole crystal is homogeneously coloured after 2 h (Figure S14). This phenomenon excludes the possibility of crystal surface loading and confirms that guest molecules can only be adsorbed and transported in these 1D channels. Pawley refinement[17] of the powder X-ray diffraction (PXRD) data for **PCS^S** after adsorbing iodine indicates that the overall structure of **PCS^S** is preserved (Figures S15 and S16). Figure 2b and Movie S1 record the time-dependent diffusion process from the initial to final state accompanied with apparent color change from light yellow to almost black. After fully loading, thermo gravimetric analysis (TGA) shows the weight capacity of iodine loading is about 33% (Figure S17). Based on the TGA result, the adsorption capacity can be calculated as 1.4 iodine molecules per **PCS** molecule or 0.51 g of iodine per gram of **PCS**. Furthermore, when one of the (001) faces of the needle crystal was sealed by immersing it in glycerol, the sublimed iodine vapor can only diffuse into the central part of the crystal through another (001) face. The gradually quenched emission starts from the unblocked entrance, further confirming the 1D porosity (Figure 2c and Movie S2).

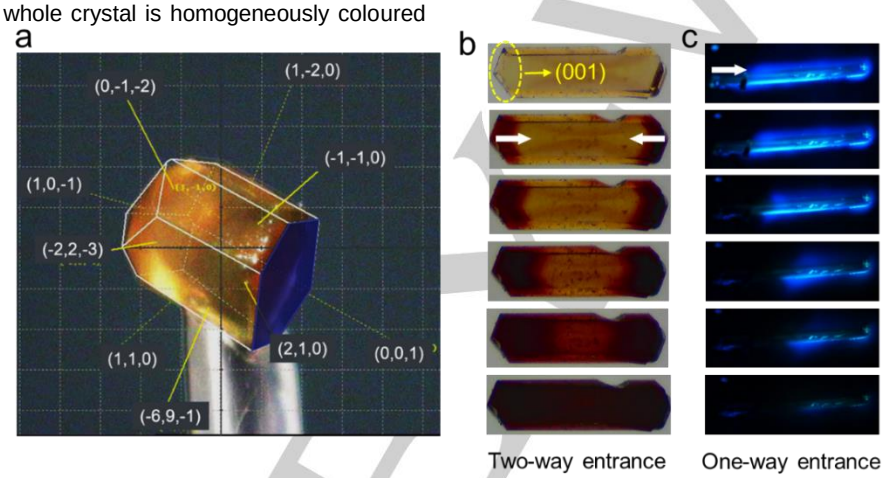

Figure 2. (a) A crystal of **PCS^S** with face-indexing graphics. The blue hexagon indicates (001) face of crystal, which is also one of the entrances of the tunnel. (b) **PCS^S** featuring different states of the process of diffusion of iodine from initial to final state. Diffusion started from the two (001) faces to the central part. (c) Fluorescence images of **PCS^S** at different diffusion states with the right capped face immersed in glycerol. Diffusion started from only the left capped (001) to the central part.

Thermal stability and SCSC Phase Transformations upon Heating. Discrete molecules tend to maximize attractive interactions and leave minimal voids as possible in their crystal packing.[18] Therefore most solvated structures do not commonly retain their incipient porosity on guest removal, but rather collapse to form a denser phase.[6a, 19] TGA profile of **PCS^S** shows multistep mass loss to reach a plateau at ca. 280 ºC and this plateau was maintained until the decomposition of the material beyond 320 °C (Figure S19). In a DSC profile from 5 to 280 ºC, the porous **PCS^S** displayed a significant broad endothermic peak around 30-100 °C in the first heating process which is attributed to the solvents loss (red curve in Figure 3a). This indicates solvents in the voids of **PCS^S** can be removed by heating to 100 °C. Notably, another single exothermic peak also appears at 220 °C which is ascribed to a crystalline phase transition.[20] Upon subsequent cooling, neither an exothermic peak nor an endothermic peak appears (blue curve in Figure 3a), indicating that the phase transition at 220 °C is irreversible and the new form (**PCS^T**) is thermodynamically more stable than **PCS^S**. To further confirm this hypothesis, variable-temperature powder XRD (PXRD) data for **PCS^S** were measured from 50 to 280 °C (Figure 3b). Its PXRD profile shows no obvious change below 140 °C. During 140 to 180 °C, broad peaks appear between 10° and 25° suggesting the loss of crystallinity. The strongest peak at 2θ = 5.80° (Figure 3b) in the PXRD pattern of **PCS^S** corresponds to the spacing of (2,-1,0) plane (d = 15.18 Å) in the trigonal lattice, and the measured diameter of the pore channel is similar to the d spacing of the (2,-1,0) plane (Figure S20). Thus, the unchanged sharp peak at 2θ = 5.80° indicates that the persistence of the tunnel structure at a temperature of up to 180 °C. The open pore structure is retained even after solvent removal, demonstrating the high thermal stability of the porous structure. Upon further heating to 220 °C, the PXRD profile of **PCS** changes abruptly and irreversibly with new peaks observed, confirming the formation of the new phase (**PCS^T**).

10.1002/anie.202013117

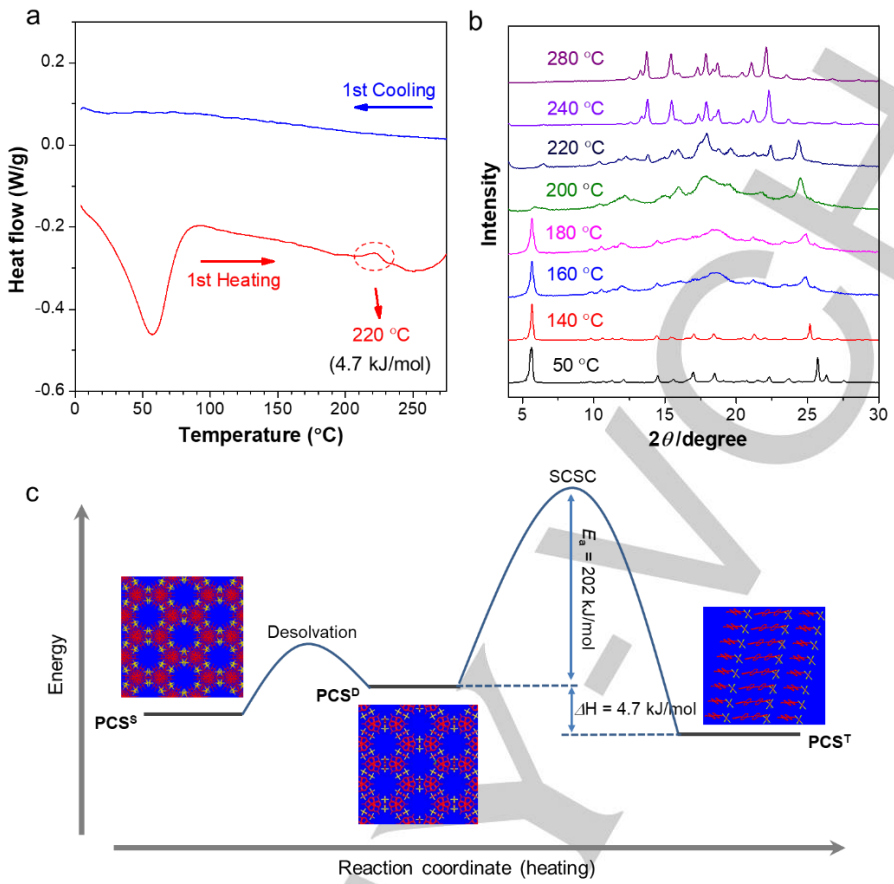

Figure 3. (a) DSC traces of **PCS^{S}** in the first heating (red curve) and first cooling (blue curve) processes (scan rate = 5 °C min^{-1}). The phase transition temperature is indicated in red dashed circle. (b) PXRD profiles of **PCS^{S}** measured at different temperatures upon heating. (c) An energy diagram for the heating process. Energy levels were estimated on the basis of the DSC profiles. Inserted are wireframe representations of the crystal-packing diagrams of **PCS^{S}**, **PCS^{D}** and **PCS^{T}**. E_a: Activation energy. **PCS^{S}** = Solvate crystal. **PCS^{D}** = Desolvated porous crystal. **PCS^{T}** = Nonporous crystal after SCSC transformation.

There is no obvious loss of crystallinity for **PCS^{S}** after desolvation at 80 °C for 15 h under vacuum. TGA analysis confirms the absence of solvent in the desolvated crystal (Figure S19). We are able to resolve the desolvated crystal structure (**PCS^{D}**), which shows almost the same pore structure with that of **PCS^{S}**. This also confirms the intermolecular interactions retained during crystal evacuation to yield a robust structure with pores (Figure 3c). Interestingly, the crystalline sample can further undergo single-crystal-to-single-crystal (SCSC) transitions at 220 °C to its nonporous polymorph (**PCS^{T}**) with enough quality for single crystal XRD analysis. This provides us concrete information about the structural transition at the molecular level. The molecular packing mode of **PCS^{S}** changes from *X*-style to *J*-style in **PCS^{T}** although their molecular conformations are similar (Figure S21). **PCS** molecules in **PCS^{T}** are connected by infinite intermolecular π-π stacking between adjacent molecules and reoriented in a slip-stack fashion with a slip angle of ≈ 35° (Figure S22). The shrink of the crystal volume indicates the packing of **PCS^{T}** is denser than that of **PCS^{S}**. It is further confirmed by the total solvent-accessible volume of **PCS^{T}**, estimated to be zero according to the *PLATON* analysis. As shown in Movie S5 and Figure S23, the closed structure of **PCS^{T}** crystal was also proven by the blockage of diffusion of I_2.

Based on the DSC and TGA profiles, a possible energy diagram for the overall crystalline transformation is proposed. It is suggested that kinetically stable **PCS^{S}** consecutively undergoes desolvation process to the solvent-free **PCS^{D}** and then the thermodynamically favorable nonporous **PCS^{T}**. The removal of solvents from **PCS^{S}** to **PCS^{D}** requires only a small activation energy, as evidenced by the TGA profile of **PCS^{S}** (Figure S19). On the other hand, a single exothermic peak associated with an enthalpy change of 4.7 kJ mol^{-1} appears at 220 °C in the DSC curve during the transformation of **PCS^{D}** to **PCS^{T}** (Figure 3a). DSC analysis with different scan rates reveals that the phase transition temperature varies with the heating rate, proving that it is indeed a kinetically enantiotropic irreversible transition. Using the Kissinger method, the activation energy for this process is calculated to be as high as 202 kJ mol^{-1}, which confirms the high thermal stability of the tunnel structure (Figure S24).

Chemical Stability and Selectivity of Gas Adsorption. Compared with the extended frameworks, porous molecular crystals formed by exclusively non-covalent bonding have less stable structures, and only a few examples of them have been reported to be stable under acidic or basic conditions.[9, 21] However, **PCS^{D}** shows surprisingly high stability toward both acid (HCl) and base (NaOH). **PCS^{D}** shows no loss of crystallinity and

10.1002/anie.202013117

no chemical decomposition when soaked in acidic (pH = 1.0) and alkaline (pH = 10) solutions for 20 h, as proved by the PXRD (Figure 4a) and ^{1}H NMR (Figure S25) results. The remarkable robustness of the tunnel can be ascribed to the strong ionic interaction with contribution of the trident anions.

Encouraged by the observed virtual porosity in the crystal structure, we examined the porosity of **PCS^D** using gas sorption measurements, including N_2, H_2, Ar, CH_4 and CO_2 (Figures 4b and S27). PXRD profiles of **PCS^D** before and after gas adsorption-desorption are consistent with that of simulated **PCS^D** and further confirm the robustness of the pore structure (Figure S26). At 77 K, **PCS^D** has a modest uptake of N_2 at 0.6 mmol/g, H_2 at 0.5 mmol/g and Ar at 1.0 mmol/g at 1 bar. The low N_2 uptake was also observed in other supramolecular organic materials with similar pore size, suggesting that N_2 molecules are unable to enter the channels at low temperature because of low kinetic energy.[4c, 6c, 10c] On the contrary, the CO_2 isotherm at 273 K shows that **PCS^D** can adsorb a decent amount of CO_2 at 2.8 mmol/g (12.3 wt%) at 1 bar. This confirms the permanent porosity of **PCS^D**. In fact, the adsorption value at 273 K has outperformed many porous hydrogen-bonded and supramolecular organic frameworks[4c, 9d, 22] , and is close to that of SOF-7a (2.85 mmol/g) under the same conditions (Table S1). The pore size distribution calculated from the CO_2 isotherm only shows one uniform pore at 7.5 Å in **PCS^D** (Figure S28), which is close to the value (6.2 Å, Figure 1b) of the channel size obtained from the crystal structure.

PCS^D uptakes a small amount of CH_4. At 1 bar, it adsorbs 0.26 mmol/g CH_4 at 273 K and 0.25 mmol at 298 K. Ideal adsorbed solution theory (IAST) was used to predict the binary adsorption of CO_2 and CH_4 mixture with 50:50 feed ratio, giving predicted CO_2/CH_4 selectivity to be 16.8 at 273 K and 7.4 at 298 K, respectively (Figure 4c).[23] To our knowledge, the selectivity at 273 K is one of the highest value in supramolecular organic frameworks reported for CO_2/CH_4 separation under the same condition (Table S1), marginally higher than that of the current best material, SOF-7a (14.2). We believed that the high polarity of the pores has contributed to the selective adsorption for CO_2. Similar behavior has also been observed in other high polarity systems.[22b] The higher quadrupole moment of CO_2 (-1.4×10^{-39} C m^2), compared with those of N_2 (4.7×10^{-40} C m^2), H_2 (2.2×10^{-40} C m^2) and CH_4 (0), suggests the enhanced electrostatic interactions between CO_2 and the charged framework, which result in higher binding affinity for CO_2.[24]

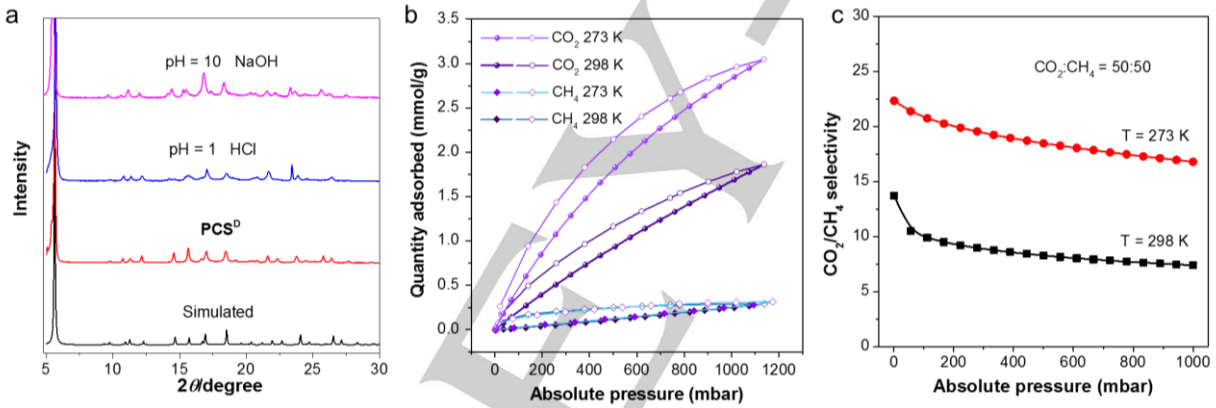

Figure 4. (a) PXRD patterns of simulated **PCS^D**, as prepared **PCS^D**, **PCS^D** in aqueous HCl (pH = 1) and NaOH (pH = 10) solutions for 20 h. (b) CH_4 (298 K), CH_4 (273 K), CO_2 (298 K) and CO_2 (273 K) adsorption isotherms of **PCS^D**. (c) CO_2/CH_4 selectivity values of **PCS^D** versus pressure calculated from a 50/50 mixture and applying IAST calculation.

Emissive Pores and Their Reversible Porosity. The inherent AIE with high sensitivity and low background noise is a useful tool to monitor the presence of guest molecules.[25] Using different solvents, we obtained six different solvated crystals, named **PCS^{S1}**-**PCS^{S6}**, with different emission wavelengths ranging from 441 to 532 nm (Figure 5a). All the six crystals have the sharp peak at $2\theta = 5.80°$ in their PXRD profiles to demonstrate the existence of 1D channels (Figure 5c). Despite the asymmetrical molecular structure of **PCS** and the presence of highly disordered solvents in **PCS^{S1}**-**PCS^{S6}**, we are able to resolve two single crystal structures from them: the aforementioned blue-green emissive **PSC^S**, herein also named as **PCS^{S3}** (474 nm) and the green emissive **PCS^{S5}** (500 nm). The simulated PXRD diagrams of **PCS^{S3}** and **PCS^{S5}** obtained from their single crystal data are almost identical patterns which suggests that they have similar crystal packing (Figure S29). This is further confirmed by the same pore along the *c*-axis of their solvated crystal structures (Figure S30). The TGA curves of the six freshly prepared samples and the associated ^{1}H NMR spectra of their solutions in DMSO-d_6 indicate that there are solvents in their voids (Figures S31, S32, S33, Table S2). X-ray crystal analysis reveals that the PF_6^- anions and the methyl groups of **PCS^{S3}** are exposed on the pore surfaces therefore can have potential interactions with guest molecules (Figure 1b). Considering the AIE characteristic of the tectons, these interactions with guest molecules further lead to responsive fluorescence change.[26] Moreover, in the solid-state, one **PCS** molecule interacts with four surrounding solvent molecules (Figure S33). All these **PCS** molecules adopt twisted conformations with different rotation angles and different distances of intermolecular hydrogen bonds/π-π interactions. Thus, the different emission of the six structures is believed to be caused by the synergy of the variation of intermolecular distances, the conformation change of the methyl groups, and solvent effects on the exposed PF_6^- ions.

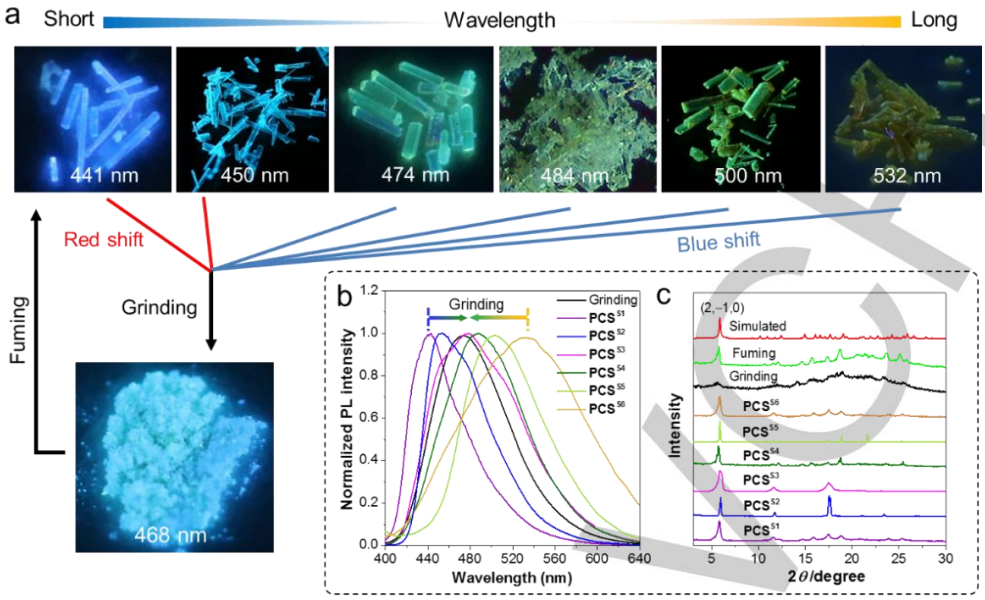

Figure 5. (a) Fluorescence images of **PCS^{S}** samples (from left to right are **PCS^{S1}** to **PCS^{S6}**) and their ground sample (bottom left). (b) Normalized PL spectra of **PCS^{S1}-PCS^{S6}** and their ground samples. (c) PXRD patterns of **PCS^{S1}-PCS^{S6}** and their corresponding ground and fumed spectra.

Non-covalent interactions endow these porous molecular crystals with dynamic behavior.[10b, 27] We found that grinding can greatly diminish the highly ordered porous structure, as suggested by the loss of crystallinity in the PXRD pattern (Figure 5c). After grinding, the emission of all **PCS** crystals shifts to 468 nm due to their transformation to the nonporous amorphous state (Figure 5a and b). By exposing the nonporous powder to dichloromethane or acetonitrile vapor, the peaks in the PXRD patterns assignable to **PCS^{S1}** are recovered (Figures 5c and S34). Therefore, we can switch the porosity in an on-off-on fashion through grinding and vapor-fuming. This reversible process is accompanied with hypochromatic or bathochromatic emission shift as suggested by the fluorescence change of the system.

Conclusion

In summary, we succeed in assembling a robust porous molecular crystal through an arrangement of strong ionic interactions and intermolecular π-π interactions from a geometrically simple molecule. The material shows good thermal stability and undergoes SCSC phase transformations in response to thermal treatment. The material exhibits exceptional chemical stability in both acidic and basic conditions, which has rarely been seen in supramolecular organic frameworks. Due to its charged tunnels, this molecular crystal also shows a large CO_2 adsorption capacity while exclusion of other gases at ambient temperature, leading to high CO_2/CH_4 selectivity which holds potential in applications such as methane purification. AIE coupled with the adaptive pores gives the crystals responsive fluorescent changes and visible on-off-on porosity transformation in the presence of external perturbation. More importantly, we believe that the linear tectons in *X*-aggregation packing mode, facilitated by ionic interactions, present a new strategy for the construction of functional porous molecular frameworks.

Experimental Section

Materials and methods, synthetic procedures, crystallographic data and characterizations are available in the supporting information.

Acknowledgements

This work was supported by the National Natural Science Foundation of China (21788102, 22001006, 81372274, 81501591 and 8141101080), the Innovation and Entrepreneurship Project of Overseas Returnees in Anhui Province (2020LCX017), the Research Grants Council of Hong Kong (16308016, C6009-17G and 16305618 and 16304819), the Innovation and Technology Commission (ITC-CNERC14SC01), the Oversea Study Program of Guangzhou Elite Project from Guangzhou City, Engineering and Physical Sciences Research Council (EP/N004884/1), and the European Research Council under the European Union's Seventh Framework Programme (FP/2007-2013)/ERC through grant agreement numbers 321156 (ERC-AG-PE5-ROBOT). We thank Dr. Marc A. Little from the University of Liverpool for helping to collect and analyse the desolvated structure. We thank Dr Yue Wu from the University of Liverpool for helping on crystal structure void analysis and discussion. We thank Dr. Kecheng Jie from the University of Cambridge for discussion on I_2 diffusion experiment.

Keywords: porous molecular crystal • linear organic salt • single-crystal-to-single-crystal transformation • CO_2 adsorption • aggregation-induced emission

[1] G. L. Verdine, *Nature* **1996**, *384*, 11-13.
[2] a) C. G. Bezzu, M. Helliwell, J. E. Warren, D. R. Allan, N. B. McKeown, *Science* **2010**, *327*, 1627-1630; b) D. Beaudoin, T. Maris, J. D. Wuest, *Nat. Chem.* **2013**, *5*, 830-834.
[3] a) R. M. Barrer, V. H. Shanson, *J. Chem. Soc. Chem. Commun.* **1976**, 333-334; b) P. Sozzani, A. Comotti, R. Simonutti, T.

Meersmann, J. W. Logan, A. Pines, *Angew. Chem. Int. Ed.*, **2000**, *39*, 2695-2699; c) J. L. Atwood, L. J. Barbour, A. Jerga, B. L. Schottel, *Science* **2002**, *298*, 1000-1002; d) P. Sozzani, S. Bracco, A. Comotti, L. Ferretti, R. Simonutti, *Angew. Chem. Int. Ed.* **2005**, *44*, 1816-1820; e) S. J. Dalgarno, P. K. Thallapally, L. J. Barbour, J. L. Atwood, *Chem. Soc. Rev.* **2007**, *36*, 236-245; f) N. B. McKeown, *J. Mater. Chem.* **2010**, *20*, 10588-10597; g) M. Mastalerz, I. M. Oppel, *Angew. Chem. Int. Ed.* **2012**, *51*, 5252-5255; h) J. Tian, P. K. Thallapally, B. P. McGrail, *CrystEngComm* **2012**, *14*, 1909-1919; i) J. Lü, R. Cao, *Angew. Chem. Int. Ed.* **2016**, *55*, 9474-9480; j) K. Jie, Y. Zhou, E. Li, F. Huang, *Acc. Chem. Res.* **2018**, *51*, 2064-2072.

[4] a) A. I. Cooper, *Angew. Chem. Int. Ed.* **2011**, *50*, 996-998; b) J. L. Atwood, L. J. Barbour, A. Jerga, *Science* **2002**, *296*, 2367-2369; c) W. Yang, A. Greenaway, X. Lin, R. Matsuda, A. J. Blake, C. Wilson, W. Lewis, P. Hubberstey, S. Kitagawa, N. R. Champness, M. Schröder, *J. Am. Chem. Soc.* **2010**, *132*, 14457-14469.

[5] a) J. D. Evans, D. M. Huang, M. Haranczyk, A. W. Thornton, C. J. Sumby, C. J. Doonan, *CrystEngComm* **2016**, *18*, 4133-4141; b) A. G. Slater, M. A. Little, A. Pulido, S. Y. Chong, D. Holden, L. Chen, C. Morgan, X. Wu, G. Cheng, R. Clowes, M. E. Briggs, T. Hasell, K. E. Jelfs, G. M. Day, A. I. Cooper, *Nat. Chem.* **2017**, *9*, 17-25.

[6] a) L. J. Barbour, *Chem. Commun.* **2006**, 1163-1168; b) P. K. Thallapally, G. O. Lloyd, J. L. Atwood, L. J. Barbour, *Angew. Chem. Int. Ed.* **2005**, *44*, 3848-3851; c) P. K. Thallapally, T. B. Wirsig, L. J. Barbour, J. L. Atwood, *Chem. Commun.* **2005**, 4420-4422; d) J. L. Atwood, L. J. Barbour, A. Jerga, *Angew. Chem. Int. Ed.* **2004**, *43*, 2948-2950; e) J. L. Atwood, L. J. Barbour, P. K. Thallapally, T. B. Wirsig, *Chem. Commun.* **2005**, 51-53; f) P. K. Thallapally, G. O. Lloyd, T. B. Wirsig, M. W. Bredenkamp, J. L. Atwood, L. J. Barbour, *Chem. Commun.* **2005**, 5272-5274.

[7] a) K.-D. Zhang, J. Tian, D. Hanifi, Y. Zhang, A. C.-H. Sue, T.-Y. Zhou, L. Zhang, X. Zhao, Y. Liu, Z.-T. Li, *J. Am. Chem. Soc.* **2013**, *135*, 17913-17918; b) I. Hisaki, C. Xin, K. Takahashi, T. Nakamura, *Angew. Chem. Int. Ed.* **2019**, *58*, 11160-11170; c) R.-B. Lin, Y. He, P. Li, H. Wang, W. Zhou, B. Chen, *Chem. Soc. Rev.* **2019**, *48*, 1362-1389; d) K. Geng, T. He, R. Liu, S. Dalapati, K. T. Tan, Z. Li, S. Tao, Y. Gong, Q. Jiang, D. Jiang, *Chem. Rev.* **2020**, *120*, 8814-8933; e) I. Bassanetti, S. Bracco, A. Comotti, M. Negroni, C. Bezuidenhout, S. Canossa, P. P. Mazzeo, L. Marchió, P. Sozzani, *J. Mater. Chem. A* **2018**, *6*, 14231-14239.

[8] R.-R. Liang, S.-Y. Jiang, R.-H. A, X. Zhao, *Chem. Soc. Rev.* **2020**, *49*, 3920-3951.

[9] a) Q.-H. Guo, Z. Liu, P. Li, D. Shen, Y. Xu, M. R. Ryder, H. Chen, C. L. Stern, C. D. Malliakas, X. Zhang, L. Zhang, Y. Qiu, Y. Shi, R. Q. Snurr, D. Philp, O. K. Farha, J. F. Stoddart, *Chem* **2019**, *5*, 2353-2364; b) H. Yamagishi, H. Sato, A. Hori, Y. Sato, R. Matsuda, K. Kato, T. Aida, *Science* **2018**, *361*, 1242-1246; c) T.-H. Chen, I. Popov, W. Kaveevivitchai, Y.-C. Chuang, Y.-S. Chen, O. Daugulis, A. J. Jacobson, O. Š. Miljanić, *Nat. Commun.* **2014**, *5*, 5131; d) J. Lü, C. Perez-Krap, M. Suyetin, N. H. Alsmail, Y. Yan, S. Yang, W. Lewis, E. Bichoutskaia, C. C. Tang, A. J. Blake, R. Cao, M. Schröder, *J. Am. Chem. Soc.* **2014**, *136*, 12828-12831.

[10] a) A. Yamamoto, S. Uehara, T. Hamada, M. Miyata, I. Hisaki, N. Tohnai, *Cryst. Growth Des.* **2012**, *12*, 4600-4606; b) A. Yamamoto, T. Hamada, I. Hisaki, M. Miyata, N. Tohnai, *Angew. Chem. Int. Ed.* **2013**, *52*, 1709-1712; c) A. Comotti, S. Bracco, A. Yamamoto, M. Beretta, T. Hirukawa, N. Tohnai, M. Miyata, P. Sozzani, *J. Am. Chem. Soc.* **2014**, *136*, 618-621; d) S. Bracco, T. Miyano, M. Negroni, I. Bassanetti, L. Marchio, P. Sozzani, N. Tohnai, A. Comotti, *Chem. Commun.* **2017**, *53*, 7776-7779.

[11] a) V. A. Russell, C. C. Evans, W. Li, M. D. Ward, *Science* **1997**, *276*, 575-579; b) T. Adachi, M. D. Ward, *Acc. Chem. Res.* **2016**, *49*, 2669-2679.

[12] a) G. Xing, T. Yan, S. Das, T. Ben, S. Qiu, *Angew. Chem. Int. Ed.* **2018**, *57*, 5345-5349; b) S. Yu, G.-L. Xing, L.-H. Chen, T. Ben, B.-L. Su, *Adv. Mater.* **2020**, *32*, 2070331.

[13] J. Mei, N. L. Leung, R. T. Kwok, J. W. Lam, B. Z. Tang, *Chem. Rev.* **2015**, *115*, 11718-11940.

[14] A. Spek, *Utrecht University, Utrecht, The Netherlands* **2003**.

[15] G. Couderc, J. Hulliger, *Chem. Soc. Rev.* **2010**, *39*, 1545-1554.

[16] B. J. Riley, J. D. Vienna, D. M. Strachan, J. S. McCloy, J. L. Jerden Jr, *J. Nucl. Mater.* **2016**, *470*, 307-326.

[17] G. Pawley, *J. Appl. Crystallogr* **1981**, *14*, 357-361.

[18] J. D. Dunitz, A. Gavezzotti, *Chem. Soc. Rev.* **2009**, *38*, 2622-2633.

[19] a) S. C. Sahoo, M. K. Panda, N. K. Nath, P. e. Naumov, *J. Am. Chem. Soc.* **2013**, *135*, 12241-12251; b) P. Brunet, M. Simard, J. D. Wuest, *J. Am. Chem. Soc.* **1997**, *119*, 2737-2738.

[20] C. Ge, J. Liu, X. Ye, Q. Han, L. Zhang, S. Cui, Q. Guo, G. Liu, Y. Liu, X. Tao, *J. Phy. Chem. C* **2018**, *122*, 15744-15752.

[21] a) F. Hu, C. Liu, M. Wu, J. Pang, F. Jiang, D. Yuan, M. Hong, *Angew. Chem. Int. Ed.* **2017**, *56*, 2101-2104; b) Q. Yin, P. Zhao, R. J. Sa, G. C. Chen, J. Lü, T. F. Liu, R. Cao, *Angew. Chem. Int. Ed.* **2018**, *130*, 7817-7822; c) B. Wang, X.-L. Lv, J. Lv, L. Ma, R.-B. Lin, H. Cui, J. Zhang, Z. Zhang, S. Xiang, B. Chen, *Chem. Commun.* **2020**, *56*, 66-69.

[22] a) P. Li, Y. He, Y. Zhao, L. Weng, H. Wang, R. Krishna, H. Wu, W. Zhou, M. O'Keeffe, Y. Han, B. Chen, *Angew. Chem. Int. Ed.*, **2015**, *54*, 574-577; b) G. Xing, I. Bassanetti, S. Bracco, M. Negroni, C. Bezuidenhout, T. Ben, P. Sozzani, A. Comotti, *Chem. Sci.* **2019**, *10*, 730-736; c) H. Wang, B. Li, H. Wu, T.-L. Hu, Z. Yao, W. Zhou, S. Xiang, B. Chen, *J. Am. Chem. Soc.* **2015**, *137*, 9963-9970; d) W. Yang, W. Zhou, B. Chen, *Cryst. Growth Des.* **2019**, *19*, 5184-5188; e) J. Lü, C. Perez-Krap, F. Trousselet, Y. Yan, N. H. Alsmail, B. Karadeniz, N. M. Jacques, W. Lewis, A. J. Blake, F.-X. Coudert, R. Cao, M. Schröder, *Cryst. Growth Des.* **2018**, *18*, 2555-2562; f) W. Yang, J. Wang, H. Wang, Z. Bao, J. C.-G. Zhao, B. Chen, *Cryst. Growth Des.* **2017**, *17*, 6132-6137.

[23] S. Lee, J. H. Lee, J. Kim, *Korean J. Chem. Eng.* **2018**, *35*, 214-221.

[24] X.-Z. Luo, X.-J. Jia, J.-H. Deng, J.-L. Zhong, H.-J. Liu, K.-J. Wang, D.-C. Zhong, *J. Am. Chem. Soc.* **2013**, *135*, 11684-11687.

[25] M. Zhang, G. Feng, Z. Song, Y.-P. Zhou, H.-Y. Chao, D. Yuan, T. T. Y. Tan, Z. Guo, Z. Hu, B. Z. Tang, B. Liu, D. Zhao, *J. Am. Chem. Soc.* **2014**, *136*, 7241-7244.

[26] B. Wang, R. He, L.-H. Xie, Z.-J. Lin, X. Zhang, J. Wang, H. Huang, Z. Zhang, K. S. Schanze, J. Zhang, S. Xiang, B. Chen, *J. Am. Chem. Soc.* **2020**, *142*, 12478-12485.

[27] Q. Huang, W. Li, Z. Mao, L. Qu, Y. Li, H. Zhang, T. Yu, Z. Yang, J. Zhao, Y. Zhang, M. P. Aldred, Z. Chi, *Nat. Commun.* **2019**, *10*, 3074.

10.1002/anie.202013117

WILEY-VCH

RESEARCH ARTICLE

A linear ionic molecule forms stable framework with open pores through *X*-aggregation packing, facilitated by a combination of trident-type ionic interactions and π-π stacking. The nano-tunnel exhibits anisotropic guest diffusion, excellent chemical stability, large CO_2 uptake with high CO_2/CH_4 selectivity, and vapochrometric behavior.

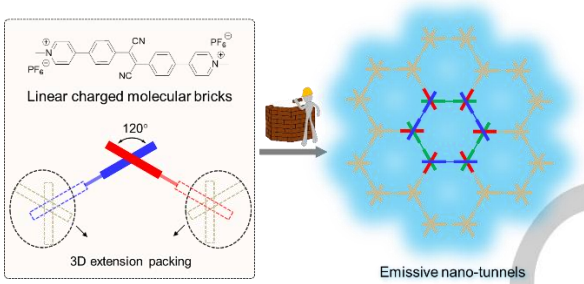

Peifa Wei, Xuan He, Zheng Zheng, Donglin He, Qiyao Li, Junyi Gong, Jun Zhang, Herman H. Y. Sung, Ian D. Williams, Jacky W. Y. Lam, Ming Liu,* and Ben Zhong Tang**

Page No. – Page No.

Robust Supramolecular Nano-tunnels Built from Molecular Bricks